NANO LETTERS

pubs.acs.org/NanoLett

Unity-Order Index Change in Transparent Conducting Oxides at Visible Frequencies

Eyal Feigenbaum,*,† Kenneth Diest,†,§ and Harry A. Atwater

Thomas J. Watson Laboratory of Applied Physics, California Institute of Technology, Pasadena, California 91125

ABSTRACT We report a method for obtaining unity-order refractive index changes in the accumulation layer of a metal-oxide-semiconductor heterostructure with conducting oxide as the active material. Under applied field, carrier concentrations at the dielectric/conducting oxide interface increase from 1×10^{21}/cm^3 to 2.8×10^{22}/cm^3, resulting in a local refractive index change of 1.39 at 800 nm. When this structure is modeled as a plasmonic waveguide, the change corresponds to a modal index change of 0.08 for the plasmonic mode.

KEYWORDS Active plasmonics, index modulation, transparent conducting oxides, indium tin oxide, electro-optical devices, waveguides

Efforts to modify the refractive index of optical materials by applying electric fields have been a constant focus in the field of photonics. These advances include the Pockels and Kerr electro-optic effects, resulting from a field-induced distortion or reorientation of the molecular and unit-cell level constituents of materials. For the Kerr effect, the refractive index change is on the order of $\Delta n_{\text{index}} \sim 10^{-2}-10^{-6}$, whereas for the Pockels effect, $\Delta n_{\text{index}} \sim 10^{-4}-10^{-6}$ is typically possible. Carrier-induced changes offer a different method of index modification. However, the carrier densities and the resulting refractive index changes are inherently small for conventional semiconductors (e.g., Si, GaAs),[1] which may be enhanced by changing the optical dispersion within the device (e.g., in ref 2 the device was designed to operate very near modal cutoff). As detailed below, conducting oxides that have carrier densities in the $10^{21}-10^{23}$/cm^3 range represent an alternative approach where changes in carrier density yield strong, that is, on the order of unity, changes in the refractive index. This effect, in combination with appropriate waveguide design, leads to a substantial change in wave propagation.

To facilitate comparison of electro-optic, carrier-induced, and thermally induced phase changes in material refractive index, we characterize each via a figure-of-merit (F.O.M.) equal to the ratio of index change to required power density. For the Kerr effect, with $\Delta n_{\text{index}} \sim 0.007$ under applied fields of $\sim 20 \times 10^{12}$ W/cm^2,[3] the FOM is $\sim 10^{-16}$ cm^2/W. Another possible approach is inducing a phase change by heating. Using a polymer layer, typical changes from this mechanism are on the order of $\Delta n_{\text{index}} \sim 10^{-4}$ with a thermal power density of 6×10^3 W/cm^2.[4] This gives a FOM of ~ 0.023 cm^2/W, which is higher than the previous example yet still relatively small. In the case of phase changes in gallium, a unity-order change to the negative real permittivity was demonstrated in a 15 nm thick layer with a thermal power density of 0.3 W/cm^2,[5] which gives a FOM of ~ 3 cm^2/W. The photorefractive effect enables index changes with a slightly higher figure of merit. In the case of lithium niobate, the index change is $\Delta n_{\text{index}} \sim 10^{-3}$ under an applied electric field of $\sim 10^5$ V/cm,[6] with a FOM of ~ 20 cm^2/W. Carrier-induced index changes in a metal−oxide−semiconductor (MOS) configuration driven into accumulation require low electronic power densities of $\sim 10^{-7}$ W/cm^2; however, based on the Drude-Lorentz relations, the maximum induced index change is limited to $\Delta n_{\text{index}} \sim 10^{-3}$ at visible frequencies,[1] and the FOM is therefore $\sim 10^4$ cm^2/W. Another limitation of this effect is that the index change is confined to the thickness of the resulting accumulation layer at the oxide-semiconductor interface. This layer thickness is typically much smaller than the modal cross-section, and as a result there is a small change in the overall modal effective index.

One solution to this problem is to design the MOS structure for usage as a plasmonic waveguide. Surface plasmon polariton modes in nanoscale waveguides give extremely high modal confinement[7−9] and have recently received considerable attention for use in nanophotonic circuit applications. More recently, index changes in these modes have been studied via thermal effects,[4,5,10] ferroelectrics,[11] two-wave interaction mediated by quantum dots[12] or molecules,[13] ultrafast changes in the electron distribution under a probe beam,[14] and carrier density variations with applied field.[2] In this Letter, we demonstrate a local Δn_{index} of ~ 1.5 in a conducting oxide with electronic power densities of $\sim 10^{-5}$ W/cm^2 corresponding to a FOM of $\sim 10^5$ cm^2/W. We also take advantage of the extremely high plasmonic modal confinement to achieve a change in the modal effective index of ~ 0.1, which corresponds to a FOM of $\sim 10^4$ cm^2/W.

* To whom correspondence should be addressed. E-mail: eyalf@caltech.edu.

† These authors have contributed equally to this manuscript.

§ Current address: Northrop Grumman Aerospace Systems, One Space Park, Redondo Beach, CA 90278.

Received for review: 02/22/2010
Published on Web: 05/18/2010

DOI: 10.1021/nl1006307 | *Nano Lett.* **2010,** *10,* 2111–2116

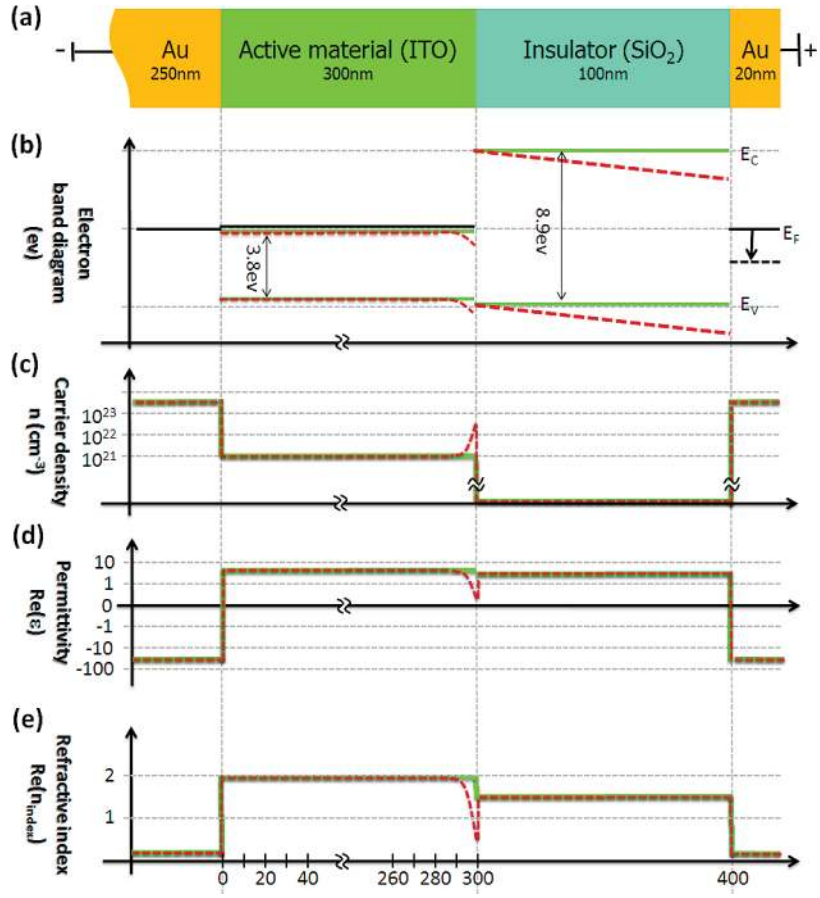

FIGURE 1. MOS structure with (dashed red) and without (solid green) charge accumulation. (a) Structure schematics. When a voltage is applied to the MOS device (the semiconductor is replaced with a higher carrier density active material) an accumulation layer forms. (b) The band diagram and (c) the carrier density are modified by an applied voltage across the insulator/active material interface, which forms an accumulation layer. (d) As the carrier density increases at the interface, this layer becomes "more metallic like" and the local permittivity is reduced. This accumulation results in a large local permittivity and (e) refractive index modulation.

A diagram of the experimental structure is shown in Figure 1. Under an applied field, the structure in Figure 1a forms an accumulation layer at the dielectric-conducting oxide interface. The resulting band diagram and excess carrier density are shown in Figure 1b,c, respectively. Figure 1d,e illustrates the intense local change in the permittivity and refractive index, respectively. The diagrams are drawn to scale based on results presented later in the Letter. A Drude-Lorentz model[1] can be used to describe the change in the complex refractive index

$$\Delta n_{\text{index}} = \frac{-e^2\lambda_0^2}{8\pi^2 c^2 \varepsilon_0 n_{\text{index}}}\left(\frac{\Delta n}{m_e^*} + \frac{\Delta p}{m_h^*}\right) \qquad (1)$$

where Δn and Δp represent the excess electron and hole densities in the accumulation layer beyond their values in equilibrium flat band conditions. The other parameters in eq 1 have their normal meaning, i.e., e is the electronic charge; λ_0 is the free space wavelength; c is the speed of light in vacuum; ε_0 is the vacuum permittivity; m_e^* and m_h^* are the respective electron and hole effective masses. For a typical semiconductor like silicon, $\Delta n = 10^{19}$ cm^{-3} is possible, giving $\Delta n_{\text{index}} = 0.002$ at $\lambda_0 = 800$ nm and $\Delta n_{\text{index}} = 0.009$ at $\lambda_0 = 1500$ nm.

The simplified Drude model shown in Figure 2 illustrates that carrier densities approaching $n = 10^{21}$ cm^{-3} are required to produce significant index changes at visible frequencies. These large index changes can alternatively be viewed as a shift in the plasma frequency toward visible frequencies with increasing carrier density. The required carrier densities are determined using the Drude model for permittivity

$$\varepsilon = \varepsilon_\infty - \frac{\omega_p^2}{\omega^2 + i\omega\Gamma}; \quad \omega_p^2 = \frac{ne^2}{\varepsilon_\infty m^*} \qquad (2)$$

where ε is the material permittivity, ε_∞ is the high frequency permittivity, ω is the angular frequency, ω_p is the plasma frequency, and Γ is the relaxation frequency. The dispersive permittivity calculated in Figure 2 assumes $\varepsilon_\Gamma = 1$, $\Gamma = 0$, and $m^* = m_e$ (the rest mass of electron). For each curve,

DOI: 10.1021/nl1006307 | *Nano Lett.* **2010,** *10,* 2111–2116

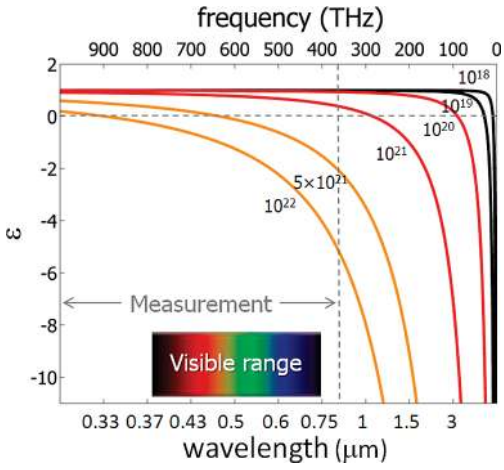

FIGURE 2. Permittivity dispersion modified by a change in the carrier concentration. As the carrier density (per cubic centimeter) increases, the plasma frequency ($\varepsilon = 0$) shifts toward visible frequencies, and the dispersion becomes substantially different in that regime. Here the Drude model (eq 2) was used with $\varepsilon_\infty = 1$, $\Gamma = 0$, $m^* = m_e$.

the plasma frequency corresponds to the point where $\varepsilon = 0$. The two black curves illustrate typical degenerately doped semiconductors. Starting with a carrier density of 10^{18} cm^{-3}, an applied voltage forms an accumulation layer with a carrier density of 10^{19} cm^{-3} and shifts the plasma frequency toward visible frequencies in that layer. However, at visible frequencies the change in permittivity between the two carrier densities is negligible. For the case of a material with an equilibrium carrier density of 10^{20} cm^{-3}, a carrier density increase to 10^{21} cm^{-3} is possible in accumulation, and corresponds to a plasma frequency shift to higher near-infrared frequencies. In this case, substantial changes in the permittivity of the accumulation layer occur at visible frequencies.

To achieve these carrier densities, we used conducting oxide thin films as the active layer within the field effect heterostructure. Both indium tin oxide (ITO) and indium zinc oxide (IZO) are degenerately doped semiconductors that are widely used as transparent electrodes in solar cells and displays.[15−17] These materials can be doped to have carrier concentrations between 10^{19}−10^{21} cm^{-3} by manipulating the concentration of oxygen vacancies and interstitial metal dopants. These high carrier densities could allow for guiding surface modes in the infrared frequencies on the interface of a conducting oxide with air.[18] At the same time, these conducting oxides can have greater than 80 % transmittance at visible frequencies for typical layer thickness of ∼300 nm.[15] The MOS configuration is ideal for exploring this effect both electrically as well as optically. Electronically, this structure supports a highly localized accumulation layer. Optically, the field effect heterostructure supports highly confined plasmonic modes that have a high spatial overlap with the accumulation layer. The heterostructure also forms a metal−insulator−metal (MIM) waveguide between the metal cladding layers, and the lowest transverse-magnetic (TM_0) mode of the MIM waveguide does not exhibit cutoff, even at extremely small dimensions.[19] Instead, the modal intensity is tightly confined between the two metal layers and the effective index of the wave (defined as the ratio of the wave propagation constant and the free space wavenumber) is higher than that of light in the waveguide core.

A layered MOS structure was fabricated with ITO as the active layer, Figure 1(a). Two Au layers form the metal contacts, and silicon dioxide (SiO_2) is used as the insulator. The bottom Au layer is an optically opaque 250 nm thick film, and the top Au layer is a semitransparent 20 nm thick film. The conducting oxide films were characterized using Hall measurements and spectroscopic ellipsometry. Hall measurements yielded a room temperature electron mobility in ITO films of $\mu = 14.5$ cm^2/V-s and an equilibrium electron concentration of $n = 5 \times 10^{20}$ cm^{-3}.

Spectroscopic ellipsometry, which is highly sensitive to index variations in layered structures, was used to measure the permittivity changes in nanoscale accumulation layers over a wavelength range from 300 to 820 nm. Modeling the refractive index using a Drude model and obtaining the electron density from self-consistent solutions to Poisson's equation; the expected permittivity change under applied voltage occurs within a ∼5 nm thick accumulation layer.

The permittivity modulation across the layered structure was determined as follows. First, ellipsometric models were obtained for each thin film (Au, SiO_2, and ITO). These results were converted to permittivity dispersion plots by fitting the data to Cauchy or Drude models. It was difficult to perform a purely Drude fit to the permittivity at wavelengths shorter than 500 nm for Au because of interband transitions and the onset of the band gap in ITO. Therefore the fit was restricted to the wavelength interval between 500−800 nm, where the Drude model is valid. Second, ellipsometry was performed on the entire heterostructure, shown in Figure 1a, until self-consistency was achieved between the complex indices in the heterostructure and the respective permittivities for each individual material. After verifying that no other sources of index modulation existed, it was assumed that the observed heterostructure refractive index change with applied field was due to the formation of an accumulation layer at the SiO_2/ITO interface. To do this, the Drude parameters of the accumulation layer and its thickness were fitted while the parameters of the other layers were held constant. For the ellipsometry measurements, the accumulation layer was modeled as a layer with uniform index and thickness equal to the decay length of the expected exponential decay profile. This assumption is justified by the expected (and experimentally resolved) accumulation layer width of a few nanometers, which is essentially a step function for the ellipsometry probing beam. The thickness of the experimentally measured accumulation layer was found to be 5 ± 1 nm for all applied voltages. Fitting Ψ and Δ for each of the layers, as well as the entire layer stack, was done by minimizing the mean-square error between the

DOI: 10.1021/nl1006307 | *Nano Lett.* **2010,** *10,* 2111--2116

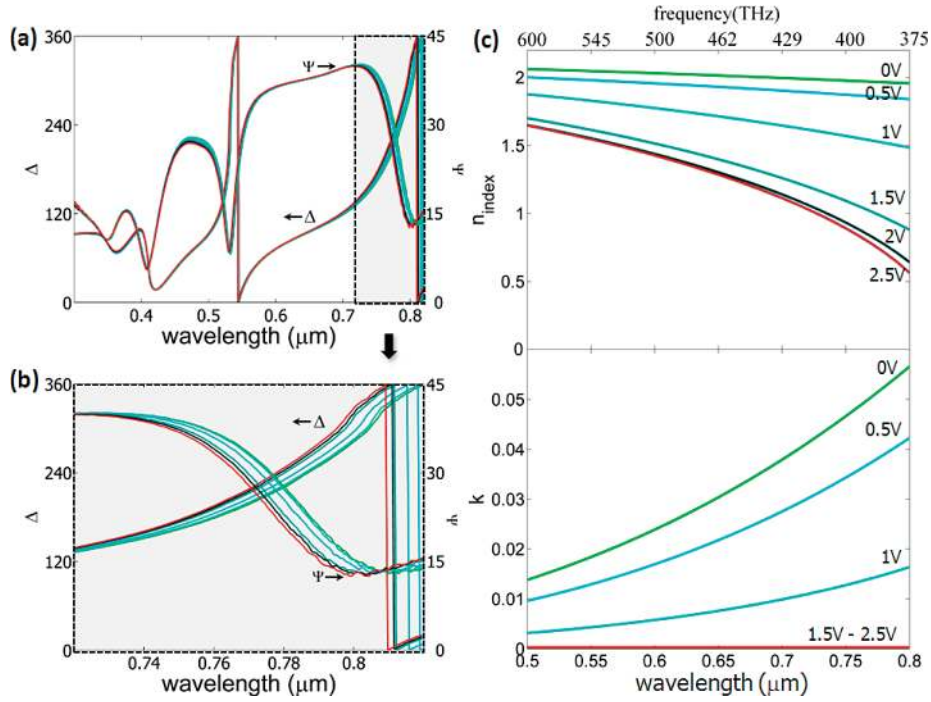

FIGURE 3. Measured modulation with applied voltage. (a) Ellipsometry (Δ and Ψ) vs wavelength for the layered stack at different applied voltages. The data is modulated with applied voltage, which is clearer after expending the 720−820 nm range, given in (b). (c) The complex refractive index in a 5 nm accumulation layer, extracted from the ellipsometry data.

TABLE 1. Accumulation Layer Properties under Voltage

voltage (V)	ε_∞	ω_p (10^{12} rad/s)	Γ (THz)	n (cm^{-3})	$\lambda_p(\varepsilon_\infty)^{1/2}$ (nm)
0	4.55	2096.8	724.6	1×10^{21}	1918
0.5	4.41	2409.3	359.7	2.72×10^{21}	1643
1	4.37	3468.7	52.9	1.65×10^{22}	1136
1.5	4.25	4392.7	0	2.57×10^{22}	885
2	4.2	4585.1	0	2.77×10^{22}	843
2.5	4.16	4671.7	0	2.83×10^{22}	823

model and measured data by varying the materials parameters. The SiO_2 film was modeled as a Cauchy layer, and the Au and ITO films were modeled using Drude layers. We validated the uniform single layer model for the accumulation layer by comparing its ellipsometry predictions with the ones of a model where the accumulation layer is represented by an exponentially decaying multilayer index, having 5 nm decay length. The comparison of the two models' data sets shows close agreement, that is, the average difference over the frequency range is 0.08% in Δ and 0.6% in Ψ when a voltage of 2.5 V is applied.

The experimental results show that the refractive index in the accumulation layer is substantially altered under an applied voltage. Ellipsometric measurements of the thin film stack are shown in Figure 3a from 0−2.5 V in 0.5 V steps. The plot shows both Ψ and Δ over the entire measured spectrum, and Figure 3b is an expanded view of Δ from 720−820 nm, showing clear peak shifting of Ψ and Δ with applied voltage. The Drude model parameters of the accumulation layer under different applied voltages are given in Table 1 where the thickness was found to be 5 ± 1 nm for all applied voltages. The equilibrium carrier density is in good agreement with the values obtained from Hall probe measurements. The relatively low gate voltages required to achieve accumulation are attributed to a nonplanar gate structure with needle-like gold filaments that protrude partially into the SiO_2, which were created during the fabrication process (see Supporting Information). The last column, $\lambda_p(\varepsilon_\infty)^{0.5}$, corresponds to the wavelength at which the real and imaginary parts of the complex refractive index become equal. This point shifts from the infrared toward the visible range as the applied voltage increases. The dispersion of these values, denoted as n_{index} and k accordingly, are depicted in Figure 3c. The measurements indicate a large change in the refractive index between 25−75%, at visible wavelengths in a 5 nm layer. For 2.5 V, at $\lambda_0 = 500$ nm the index change is $\Delta n_{index} = 0.41$ and at $\lambda_0 = 800$ nm the index change is $\Delta n_{index} = 1.39$. This change in index is accompanied by an increase in the carrier concentration from 10^{21} to 10^{22} cm^{-3}. The imaginary part of the refractive index with and without applied electric field is negligible in this wavelength range and therefore plotted in a different vertical scale than the real part.

Further studies of conducting oxide field effect heterostructres also support the plasma frequency and refractive index modulation being attributable to carrier accumulation. The effect was not observed when a negative voltage was applied to the top, semitransparent electrode, since negative voltages result in depletion layer formation. When the thickness of the SiO_2 was doubled, the index change was reduced by approximately a factor of 2 for a given voltage,

DOI: 10.1021/nl1006307 | *Nano Lett.* **2010,** *10,* 2111--2116

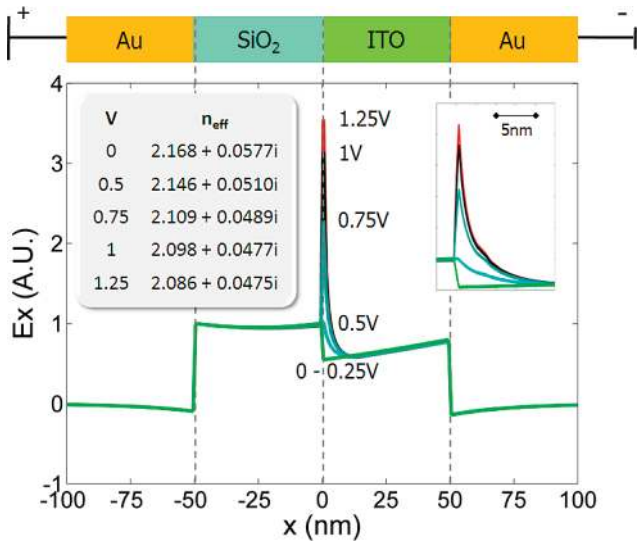

FIGURE 4. TM_0 mode profile with and without an applied voltage. The transverse electric field distribution is plotted as function of the applied voltage. The voltage is scaled down by a factor of 2 from the experiment with the SiO_2 layer. The 1.25 V applied voltage corresponds to a change of 0.08 in the modal effective index.

since the capacitance was reduced. Moreover, the same degree of refractive index modulation was observed when the thickness of the ITO layer was decreased by half, consistent with the fact that such an ITO layer thickness change would not affect the accumulation layer. In addition, no refractive index modulation was observed unless the SiO_2 layer was present, which is necessary to form an accumulation layer. Finally, for similar carrier concentrations, the same effect was also observed in heterostructures with IZO conducting oxide films. All of the above indicate that the origin of refractive index change is related to the formation of an accumulation layer at the SiO_2/conducting oxide interface.

Finally, we point out that modulation of the local refractive index within these structures, combined with the high modal confinement achievable in plasmonic waveguides, could produce large changes in the mode effective index of propagating plasmonic modes. Figure 4 shows the TM_0 mode profiles at $\lambda = 800$ nm in a MIM waveguide created by the heterostructure. Here the SiO_2 and ITO layers are both 50 nm thick and the mode profile is shown with and without an applied voltage. Under applied voltage, a significant portion of the optical mode resides at the SiO_2/ITO interface, within the accumulation layer. In the modal analysis, we used an exponential decay profile for the refractive index in the accumulation layer with the experimentally determined 5 nm decay length. We used the more detailed index profile of the accumulation layer in this analysis, since the highly confined plasmonic mode is sensitive to index variations over even few nanometers of its cross-section. The mode refractive index values are based on the results shown in Figure 3 and we used the Drude model to calculate the refractive index profile of the accumulation layer. To represent the refractive index of the spatially varying charge distribution calculated from the Poisson equation, the accumulation layer is modeled as multiple 1 nm thick Drude layers of varying conductivity with maximal plasma frequency corresponding to the values in Table 1 and a decay length of $t = 5$ nm. With no applied voltage, the mode has an effective index of $n_{eff} = 2.168 + 0.0577i$. With an applied voltage of 2.5 V, the mode effective index has changed to $n_{eff} = 2.086 + 0.0475i$. This corresponds to a change of $\Delta n_{eff} = 0.083$ (0.09 according to the step profile change), corresponding to a change of ~3.8% in the modal propagation constant at 800 nm. Such an index modulation is capable of producing a π-phase shift after only 4.8 μm of propagation, which could be used to design ultracompact, interference-based modulators.[20]

In this work we obtained a unity-order localized change in the index of refraction at visible frequencies by shifting the plasma frequency of accumulation layers within conductive oxides. The study was based on ellipsometry measurements of a MOS heterostructure with conductive oxides as the active layer. Under an applied field, the accumulation layer was shown to induce a substantial change in the local index of refraction. The heterostructure was also modeled as an MIM waveguide, and modal analysis showed that this intense, yet localized change would produce a substantial change in the modal refractive index. Future studies of this effect will focus on the time-dynamics of the accumulation layer formation as well as using this to design integrated plasmonic devices. We believe that the results shown here have the potential to open new avenues for nanoplasmonic circuitry utilizing semimetals as active waveguiding materials.

METHODS

For all experiments, ITO and IZO conducting oxide films were deposited using RF magnetron sputtering in an oxygen/argon plasma. All depositions were done at room temperature and at 3 mTorr pressure within the chamber. For conducting oxide depositions, the gas during sputtering was 1.29% O_2 and 98.71% Ar, and the films were sputtered at 200 W. The targets used were $(In_2O_3)_{0.9}(ZnO)_{0.1}$, and $(In_2O_3)_{0.9}(SnO)_{0.1}$ weight percent. For SiO_2 depositions, the gas during sputtering was 28.45% O_2 and 71.55% Ar, and the films were sputtered at 224 W. All gold films were deposited using thermal evaporation. For Hall probe measurements, films of ITO were deposited on quartz slides.

Acknowledgment. We thank S. Burgos, A. Leenheer, D. O'Carroll, G. Kimball, and G. Miller for engaging discussions and technical assistance. We acknowledge support by the Office of Basic Energy Sciences under Contract Number DOE DE-FG02-07ER46405 and under the Air Force Office of Scientific Research under Grant FA9550-09-1-0673. E.F. acknowledges fellowship support from the Rothschild Foundation.

DOI: 10.1021/nl1006307 | *Nano Lett.* **2010,** *10,* 2111–2116

Supporting Information Available. SEM image and figure of electrostatic caluculation. This material is available free of charge via the Internet at http://pubs.acs.org.

REFERENCES AND NOTES

(1) Reed, G. T.; Jason Png, C. E. *Mater. Today* **2005**, 40–50.
(2) Dionne, J. A.; Diest, K.; Sweatlock, L. A.; Atwater, H. A. *Nano Lett.* **2009**, *9*, 897–902.
(3) Aitchison, J. S.; Weiner, A. M.; Silberberg, Y.; Oliver, M. K.; Jackel, J. L.; Leaird, D. E.; Vogel, E. M.; Smith, P. W. E. *Opt. Lett.* **1990**, *15*, 471–473.
(4) Nikolajsen, T.; Leosson, K.; Bozhevolnyi, S. I. *Appl. Phys. Lett.* **2004**, *85*, 5833–5835.
(5) Krasavin, A. V.; Zheludev, N. I. *Appl. Phys. Lett.* **2004**, *84*, 1416–1418.
(6) Valley, G. C.; Segev, M.; Crosignani, B.; Yariv, A.; Fejer, M. M.; Bashaw, M. C. *Phys. Rev. A* **1994**, *50*, R4457–R4460.
(7) Barnes, W. L.; Dereux, A.; Ebbesen, T. W. *Nature* **2003**, *424*, 824–830.
(8) Maier, S. A.; Atwater, H. A. *J. Appl. Phys.* **2005**, *98*, No. 011101.
(9) Ozbay, E. *Science* **2006**, *311*, 189–193.
(10) Lereu, A. L.; Passian, A.; Goudonnet, J.-P.; Thundat, T.; Ferrell, T. L. *Appl. Phys. Lett.* **2005**, *86*, 154101.
(11) Liu, S. W.; Xiao, M. *Appl. Phys. Lett.* **2006**, *88*, 143512.
(12) Pacifici, D.; Lezec, H. J.; Atwater, H. A. *Nat. Photon.* **2007**, *1*, 402–406.
(13) Pala, R. A.; Shimizu, K. T.; Melosh, N. A.; Brongersma, M. L. *Nano Lett.* **2008**, *8*, 1506–1510.
(14) MacDonald, K. F.; Sámson, Z. L.; Stockman, M. I.; Zheludev, N. I. *Nat. Photon.* **2008**, *3*, 55–58.
(15) Hamberg, I.; Granqvist, C. G. *J. Appl. Phys.* **1986**, R123–R159.
(16) Gordon, R. G. *MRS Bull.* **2000**, 52–57.
(17) Coutts, T. J.; Young, D. L.; Li, X. *MRS Bull.* **2000**, 58–65.
(18) West, P. R.; Ishii, S.; Naik, G. V.; Emani, N. K.; Shalaev, V. M.; Boltasseva, A. *Laser Photon. Rev.* **2010**, 1–13.
(19) Feigenbaum, E.; Orenstein, M. *IEEE J. Lightwave Tech.* **2007**, *25*, 2547–2562.
(20) Lipson, M. *IEEE J. Sel. Top. Quant.* **2006**, *12*, 1520–1526.

DOI: 10.1021/nl1006307 | *Nano Lett.* **2010,** *10,* 2111–2116